THE JOURNAL OF BIOLOGICAL CHEMISTRY VOL. 285, NO. 24, pp. 18794–18805, June 11, 2010

Polycystin-2 Activation by Inositol 1,4,5-Trisphosphate-induced Ca^{2+} Release Requires Its Direct Association with the Inositol 1,4,5-Trisphosphate Receptor in a Signaling Microdomain*[S]

Received for publication, December 2, 2009, and in revised form, April 6, 2010 Published, JBC Papers in Press, April 7, 2010, DOI 10.1074/jbc.M109.090662

Eva Sammels[‡1], Benoit Devogelaere[‡2], Djalila Mekahli[‡], Geert Bultynck[‡], Ludwig Missiaen[‡], Jan B. Parys[‡], Yiqiang Cai[§], Stefan Somlo[§], and Humbert De Smedt[‡3]

From the [‡]Department of Molecular Cell Biology, Laboratory of Molecular and Cellular Signaling, K.U. Leuven, Campus Gasthuisberg O&N1, Herestraat 49 bus 802, B-3000 Leuven, Belgium and the [§]Department of Internal Medicine, Section of Nephrology, Yale University School of Medicine, New Haven, Connecticut 06510

Autosomal dominant polycystic kidney disease is characterized by the loss-of-function of a signaling complex involving polycystin-1 and polycystin-2 (TRPP2, an ion channel of the TRP superfamily), resulting in a disturbance in intracellular Ca^{2+} signaling. Here, we identified the molecular determinants of the interaction between TRPP2 and the inositol 1,4,5-trisphosphate receptor (IP_3R), an intracellular Ca^{2+} channel in the endoplasmic reticulum. Glutathione *S*-transferase pulldown experiments combined with mutational analysis led to the identification of an acidic cluster in the C-terminal cytoplasmic tail of TRPP2 and a cluster of positively charged residues in the N-terminal ligand-binding domain of the IP_3R as directly responsible for the interaction. To investigate the functional relevance of TRPP2 in the endoplasmic reticulum, we re-introduced the protein in $TRPP2^{-/-}$ mouse renal epithelial cells using an adenoviral expression system. The presence of TRPP2 resulted in an increased agonist-induced intracellular Ca^{2+} release in intact cells and IP_3-induced Ca^{2+} release in permeabilized cells. Using pathological mutants of TRPP2, R740X and D509V, and competing peptides, we demonstrated that TRPP2 amplified the Ca^{2+} signal by a local Ca^{2+}-induced Ca^{2+}-release mechanism, which only occurred in the presence of the TRPP2-IP_3R interaction, and not via altered IP_3R channel activity. Moreover, our results indicate that this interaction was instrumental in the formation of Ca^{2+} microdomains necessary for initiating Ca^{2+}-induced Ca^{2+} release. The data strongly suggest that defects in this mechanism may account for the altered Ca^{2+} signaling associated with pathological TRPP2 mutations and therefore contribute to the development of autosomal dominant polycystic kidney disease.

Autosomal dominant polycystic kidney disease (ADPKD)[4] is an inherited human disorder that affects more than six million people worldwide and is the most common monogenic cause of kidney failure in humans (1). ADPKD results in end-stage renal disease in ~50% of the affected individuals by the age of 60. ADPKD arises as a consequence of mutations of two genes *PKD1* and *PKD2*, encoding integral membrane proteins polycystin-1 (PKD1, ~460 kDa) and polycystin-2 (TRPP2, ~110 kDa), respectively. Most mutations identified in affected families appear to truncate and (or) inactivate either of both proteins (2–5). Mutations in *PKD1* account for the vast majority (~85%) of patients with ADPKD and are associated with a more severe clinical presentation and earlier onset of end-stage renal disease than the *PKD2* phenotype (4). However, in all other aspects, *PKD1* and *PKD2* mutations produce virtually indistinguishable disease manifestations, indicating that the two proteins might function in a common signaling pathway involved in maintaining the terminally differentiated state of renal epithelial cells.

TRPP2 is a 968-amino acid (aa) protein with six predicted transmembrane domains and is highly conserved among multicellular organisms and widely expressed in various tissues (2). Structural analyses indicate that TRPP2 contains several functional domains in its C-terminal tail. There are two Ca^{2+}-binding sites (aa 680–796) arranged in a typical and an atypical EF-hand motif, which could be involved in a Ca^{2+}-mediated regulation of TRPP2 (6). An endoplasmic reticulum (ER) retention signal (aa 787–820) (7) and a coiled-coil domain (aa 839–919), responsible for homo- and heterodimerization (8, 9), are also present. Recently, it was reported that this coiled-coil domain was responsible for formation of a TRPP2 trimer that interacts with PKD1 in the plasma membrane (9).

* This work was supported in part by Grant GOA/09/012 from the Concerted Actions of the K.U. Leuven (to L. M., H. D. S., and J. B. P.), Grant G.0210.03 from the Flemish National Science Foundation (to H. D. S. and J. B. P.), and Grant P6/28 from the Interuniversity Attraction Poles Programme (to H. D. S., L. M., and J. B. P.).

[S] The on-line version of this article (available at http://www.jbc.org) contains supplemental Figs. S1–S7.

[1] Recipient of Ph.D. fellowship Grant EF95/010 from the Research Council of the K.U. Leuven (to H. D. S.).

[2] Present address: Tibotec BVBA, General De Wittelaan L11 B3, B-2800 Mechelen, Belgium.

[3] To whom correspondence should be addressed. E-mail: humbert.desmedt@med.kuleuven.be.

[4] The abbreviations used are: ADPKD, autosomal dominant polycystic kidney disease; AC, acidic cluster; CICR, Ca^{2+}-induced Ca^{2+} release; $[Ca^{2+}]_{ER}$, Ca^{2+} concentration in the ER; $[Ca^{2+}]_{cyt}$, cytosolic Ca^{2+} concentration; ER, endoplasmic reticulum; IP_3R, inositol 1,4,5-trisphosphate receptor; IICR, inositol 1,4,5-trisphosphate-induced Ca^{2+} release; LBD, ligand-binding domain; PKD1, polycystin-1; RyR, ryanodine receptor; TG, thapsigargin; TRPP2, polycystin-2; aa, amino acid(s); MOPS, 4-morpholinepropanesulfonic acid; Pipes, 1,4-piperazinediethanesulfonic acid; BisTris, 2-[bis(2-hydroxyethyl)amino]-2-(hydroxymethyl)propane-1,3-diol; GST, glutathione *S*-transferase; TBS, Tris-buffered saline; CT, C-terminal; NT, N-terminal; BAPTA, 1,2-bis(2-aminophenoxyl)ethane-*N*,*N*-*N*′,*N*′-tetraacetic acid.

There is a long-standing debate on the subcellular localization of TRPP2. TRPP2 has been detected (i) in the plasma membrane, where it is supposed to form a receptor-operated, non-selective cation channel (10), (ii) in the primary cilium, where it could act as a mechanosensitive channel, possibly in association with PKD1 (11), TRPC1 (12, 13), or TRPV4 (11, 14), (iii) in the ER, where it is proposed to function as an intracellular Ca^{2+}-release channel (15), but also in centrosomes and mitotic spindles of dividing cells (reviewed in Refs. 16–18). The trafficking of TRPP2 to these specific subcellular compartments is regulated by (i) specific motifs within the protein (7, 19), (ii) multiple protein-protein interactions, *e.g.* with phosphofurin acidic cluster sorting proteins 1 and 2 (20), and (iii) a casein kinase 2-mediated phosphorylation of Ser^{812} in the C terminus of TRPP2 (20, 21). However, the predominant subcellular localization of TRPP2 is in the ER, as shown by sensitivity to Endo H, immunofluorescence, co-localization, and co-distribution with ER-resident proteins (7, 15).

Interaction between TRPP2 and the two major intracellular Ca^{2+}-release channels, the ryanodine receptor (RyR), and the inositol 1,4,5-trisphosphate receptor (IP_3R), has been reported. Biochemical and functional assays have demonstrated that the N-terminal part of TRPP2 is sufficient to bind the cardiac RyR2, whereas the C-terminal part of TRPP2 can only bind to RyR2 when it is in the open state, thereby inhibiting RyR function (22). Co-immunoprecipitation assays indicated that TRPP2 physically interacts with the IP_3R1, most likely through its C-terminal part (23). Recently Li *et al.* (24) demonstrated also that ER-localized PKD1 can interact with the IP_3R, thereby inhibiting IP_3-induced Ca^{2+} release (IICR). Several studies observed an enhancement of intracellular Ca^{2+} release that was attributed to an effect of TRPP2 (15, 23, 25, 26), but the physiological mechanism of action was not elucidated. On the other hand, Wegierski and co-workers (27) observed that TRPP2 could also act as a passive Ca^{2+}-leak channel in the ER, thereby lowering the Ca^{2+} concentration in the ER ($[Ca^{2+}]_{ER}$), which resulted in an opposite effect and decreased the magnitude of IICR. These controversial results illustrate that the exact mechanism through which polycystins in general and TRPP2 in particular modulate Ca^{2+} signaling is not yet understood. We therefore performed a detailed analysis of the molecular and functional relationship between the IP_3R and TRPP2.

Here, we identified a conserved positively charged cluster in the N-terminal suppressor domain of the IP_3R and an acidic cluster located at the end of the ER-retention signal in the C-terminal tail of TRPP2 as being crucial for the interaction between both proteins. Moreover, in a background of renal epithelial $TRPP2^{-/-}$ cells, we observed a clear potentiation of both ATP-induced intracellular Ca^{2+} release in intact cells and IICR in permeabilized cells upon TRPP2 re-introduction. Further analysis using pathological mutants of TRPP2 and peptides that compete with the interaction between TRPP2 and the IP_3R revealed that the observed increase in IICR required both a functional TRPP2 channel and a physical interaction with the IP_3R. We suggest that TRPP2 functions as a tightly regulated channel in the ER that participates in an intracellular signaling complex together with the IP_3R, thereby stimulating intracellular Ca^{2+} release within a microdomain in the immediate neighborhood of these interacting proteins.

EXPERIMENTAL PROCEDURES

Materials—Isopropyl β-D-thiogalactoside, bovine serum albumin, carbonyl cyanide 4-trifluoromethoxyphenylhydrazone, IP_3, and ionomycin were from Sigma. Fura2-AM was from TEFlabs (Austin, TX). MagFluo4-AM, nickel-nitrilotriacetic acid-agarose resin, NuPAGE® gels, NuPAGE loading dye solution sample buffer, MOPS buffer, the Virapower kit, geneticin, all cell culture media, and supplements were from Invitrogen. ATP was from Roche Applied Science. Thapsigargin (TG) was from Alexis (Zandhoven, Belgium). Glutathione-Sepharose 4B, secondary antibodies coupled to horseradish peroxidase, Enhanced Chemiluminescence (ECL) reagents, and Hyperfilms were from GE Healthcare. r-Protein A-TSK resin was from Affiland (Liège, Belgium). Immobilon-P polyvinylidene fluoride microporous transfer membranes were from Millipore (Billerica, MA). 96-Well culture plates (CELLSTAR, black polystyrene, μClear flat bottom with lid) were from Greiner (Wemmel, Belgium). The QuikChange Site-directed Mutagenesis kit was from Stratagene (La Jolla, CA). Slide-A-Lyzer dialysis cassettes and peptides were from Thermo Fisher Scientific (Ulm, Germany). Peptides were synthesized with a purity of >70% and verified by mass spectrometry and high pressure liquid chromatography.

DNA Constructs and Adenovirus Construction—The original cDNA of mouse wild-type TRPP2, which was subcloned in a pcINeo/IRES-GFP vector with a C-terminal myc tag, was a kind gift from Dr. V. Gerke, University of Münster, Germany. Using this construct we generated an LLC-PK1 cell line (porcine renal epithelial cells) stably expressing wild-type TRPP2 by geneticin selection and subsequent fluorescence-activated cell sorter selection of a green fluorescent protein-expressing cell population.

An adenovirus was produced using the Virapower kit from Invitrogen for wild-type TRPP2 and two pathological mutants D509V and R740X. A control virus was made starting from the empty pAD/PL-DEST vector. Using Gateway technology first a pDONR221-TRPP2 wild-type construct under control of a cytomegalovirus promoter was made via a BP recombination reaction (between *att*B- and *att*P-containing substrates). Subsequently an LR recombination reaction (between *att*L- and *att*R-containing substrates) was performed to obtain destination vector pAd/PL-DEST-TRPP2. These were then transfected using Lipofectamine in HEK 293A cells, which were genetically modified and include human adenovirus type-5 DNA, to facilitate production of adenovirus. The TRPP2 D509V and R740X mutants were made by site-directed mutagenesis by introducing GTT (V) to replace GAT (D) at codon 509, and TAG (Stop) to replace CGG (R) at codon 740, respectively, with wild-type pDONR221-TRPP2 as donor DNA. The different domains of the IP_3R1 (domains 1 to 6), the complete ligand-binding domain (LBD, aa 1–604), and the suppressor domains (aa 1–225) of IP_3R1 and IP_3R3 were subcloned in the bacterial pGEX-6p2 vector with an N-terminal glutathione *S*-transferase (GST) tag, as previously described (28, 29).

The cDNA fragments corresponding to the complete cytosolic N terminus (TRPP2-NT, aa 1–221) and C terminus (TRPP2-CT, aa 679–966) of TRPP2 were subcloned into the bacterial pET21b and pGEX-6p2 vector, to obtain HIS- or GST-tagged proteins, respectively. All constructs were sequenced on a Genetic Analyzer 3100 using Big Dye Terminator V1.1 technology (Applied Biosystems, Foster City, CA).

Cell Culture—$TRPP2^{-/-}$ (2D2) renal proximal tubulus epithelial cells were derived from a $TRPP2^{-/WS25}$ mouse, transgenic for the SV40 large T-antigen (30). The cells were isolated and cultured as previously described (31). Cells were transduced by adding the adenovirus to the normal cell culture medium. For transduction of the cells, viral titers were determined for wild-type TRPP2 (1/1000), TRPP2 D509V (1/704), and TRPP2 R740X (1/1124) to obtain an equal amount of protein expression, as assayed by Western blotting. We chose in all functional experiments a moderate overexpression using the adenoviral system, mimicking endogenous levels in wild-type kidney cells instead of a massive overexpression of the protein, to avoid induction of ER stress responses.

Antibodies—For wild-type TRPP2, a mouse monoclonal antibody (sc-28331) (Santa Cruz Biotechnology Inc., Santa Cruz, CA) directed against its C-terminal tail (aa 689–968) was used at a dilution of 1/1000 in Western blotting analysis. Additionally, a rabbit polyclonal antibody directed against the N terminus (aa 103–203) (YCB9) was a kind gift from Dr. Cai and Dr. Somlo and was used to recognize wild-type TRPP2 and the D509V and R740X mutants (7). This antibody was used at a 1/5000 dilution for Western blotting analysis and 1/500 dilution for immunofluorescence. The mouse monoclonal antibody (610312) that specifically recognizes IP_3R3 (aa 22–230) was from BD Biosciences (Pharmingen), and used at a 1/1000 dilution in Western blotting. Immunological detection of IP_3R1 was carried out using a Rbt03 polyclonal antibody raised against C-terminal amino acids 2735–2749 of mouse IP_3R1 (32), at a 1/3000 dilution in Western blotting. For immunological detection of the recombinant HIS fusion proteins, a horseradish peroxidase-conjugated Penta-HIS antibody was used from Qiagen (Venlo, The Netherlands).

Immunoprecipitation—LLC-PK1 cells stably expressing wild-type TRPP2 were lysed in lysis buffer (50 mM Tris, 0.3 M NaCl, 1% Triton, 0.5 mM dithiothreitol, 0.5 mM phenylmethylsulfonyl fluoride, 0.5 mM benzamidine, 5 μM leupeptin, pH 7.5). The lysate (200 μg/sample) was cleared by centrifugation (5 min, 10,000 $\times$ *g*, 4 °C). Supernatants were incubated for 90 min at 4 °C while gently mixing (1400 rpm) with antibodies (~1.5 μg): (i) anti-TRPP2 (Santa Cruz Biotechnology Inc.), (ii) anti-IP_3R1, (iii) anti-IP_3R3, (iv) nonspecific mouse IgG (Santa Cruz Biotechnology Inc., sc-2025), or (v) nonspecific rabbit IgG (Santa Cruz Biotechnology Inc., sc-2027). Subsequently, r-protein A-TSK-Sepharose resin (50% in lysis buffer) was added and incubation was continued for another hour. Beads were collected by centrifugation (20 s, 2000 $\times$ *g*) and washed once with Tris-buffered saline (TBS) supplemented with 0.25% Triton X-100 and 0.1 M LiCl and three times with TBS supplemented with 0.25% Triton X-100. Finally, the beads were resuspended in 30 μl of NuPAGE loading dye solution sample buffer and heated for 10 min at 75 °C. Supernatants were further analyzed by SDS-PAGE and Western blotting.

Preparation of GST or HIS Fusion Proteins—pGEX-6p2 and pET21b constructs were transformed into BL21 *Escherichia-coli*. Colonies were grown overnight in 50 ml of dYT medium (16 g/liter of peptone, 10 g/liter of yeast extract, 5 g/liter of NaCl, pH 7.4) at 37 °C. dYT medium (~400 ml) was added to this preculture, and bacteria were further grown at 28 °C until A_{600} reached 0.8–1. Protein expression was induced by adding 0.1 mM isopropyl β-D-thiogalactoside and bacteria were further grown at 28 °C for 4–8 h or at 14 °C for 20 h. Bacterial cells were harvested and lysed by sonication (9 $\times$ 10 s, 12 kHz). Lysates were cleared by centrifugation (30 min, 15,000 $\times$ *g*). The soluble fractions were then incubated during 2 h with glutathione-Sepharose 4B or nickel-nitrilotriacetic acid-agarose beads at 4 °C. After washing the beads, fusion proteins were eluted with 10 mM glutathione or 250 mM imidazole, respectively. Purified proteins were dialyzed overnight against TBS, using Slide-A-Lyzer dialysis cassettes with a cut-off of 10 kDa.

GST Pulldown—Purified and dialyzed GST fusion proteins or parental GST (control) were incubated with purified and dialyzed HIS fusion proteins or a cleared lysate from LLC-PK1 cells expressing TRPP2 in pulldown buffer (50 mM Tris, 1 mM EGTA, pH 7.4) and immobilized on glutathione-Sepharose 4B beads via rotation in a head-over-head rotator for 1–2 h at 4 °C. The beads were washed 4 times with pulldown buffer and complexed GST fusion proteins were eluted in 100 mM glutathione in pulldown buffer. Eluates were further analyzed using SDS-PAGE and Western blotting.

SDS-PAGE and Western Blotting—Protein samples were analyzed by NuPAGE 4–12% BisTris SDS-polyacrylamide gels using MOPS buffer. After semi-dry electroblotting onto a polyvinylidene fluoride membrane, blocking with TBS containing 0.1% Tween and 5% nonfat dry milk powder or bovine serum albumin, and incubation with primary antibody (in TBS supplemented with 0.1% Tween and 1% nonfat dry milk powder), the blots were incubated with the horseradish peroxidase-conjugated secondary antibodies (in TBS supplemented with 0.1% Tween and 1% nonfat dry milk powder). The immunoreactive bands were visualized with ECL substrate and exposed to Hyperfilm. The Hyperfilm was developed using a Kodak X-Omat 1000 (Kodak). Total protein content was visualized by Ponceau red staining of the blot after film development. Quantification was done with ImageJ software (rsbweb.nih.gov/ij/).

$[Ca^{2+}]$ Measurements—For measurements of the free cytosolic $[Ca^{2+}]$ ($[Ca^{2+}]_{cyt}$) in intact cells, the cells were loaded with Fura2-AM (1.25 μM) in modified Krebs buffer (130 mM NaCl, 4.7 mM KCl, 1.2 mM $MgCl_2$, 1.5 mM $CaCl_2$, 10 mM glucose, 10 mM Hepes, pH 7.4) for 45 min at room temperature. This solution was then replaced by a modified Krebs buffer without Ca^{2+} indicator and the incubation continued for 30–45 min, to allow de-esterification of the loaded dye. 3 mM EGTA was added before each measurement to buffer all free extracellular Ca^{2+}. Subsequently, agonist (ATP) or 1 μM ionomycin were added to induce Ca^{2+} release from intracellular stores. Fluorescence emission was measured at 510 nm with excitation at 340/380 nm. $[Ca^{2+}]_{cyt}$ was derived after *in situ* calibration according to the following equation: $[Ca^{2+}]_{cyt}$ (nM) $= K_d \times Q \times (R - R_{min})/$

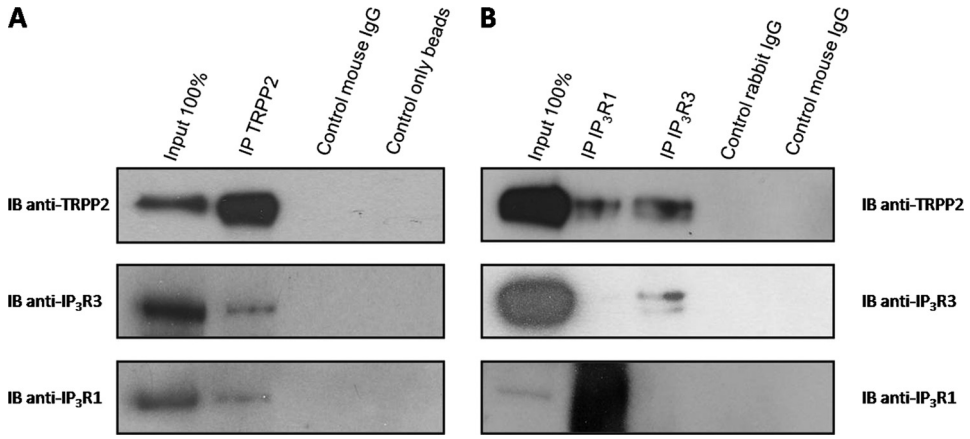

FIGURE 1. **Co-immunoprecipitation of full-length TRPP2 and IP_3R.** *A,* co-immunoprecipitation (*IP*) of endogenous IP_3R3 and IP_3R1 with TRPP2 in TRPP2-expressing LLC-PK1 cells. The *upper* immunoblot (*IB*) shows the staining for TRPP2, whereas the *lower* immunoblots show the staining for IP_3R3 and IP_3R1. *B,* co-immunoprecipitation of TRPP2 with endogenous IP_3R1 or IP_3R3. The *upper* immunoblot shows the staining for TRPP2, the *middle* immunoblot shows the staining for IP_3R3 and the *lower* immunoblot shows the staining for IP_3R1. Representative immunoblots from three independent experiments are shown.

($R_{max} - R$); K_d is the dissociation constant of Fura2 for Ca^{2+} at room temperature (220 nM), Q is the fluorescence ratio of the emission intensity excited by 380 nm in the absence of Ca^{2+} to that during the presence of saturating Ca^{2+}, R is the fluorescence ratio, R_{min} and R_{max} are the minimal and maximal fluorescence ratios, respectively. R_{min} was measured by perfusion with 10 mM EGTA in Ca^{2+}-free Krebs solution and R_{max} was obtained by perfusion with 5 μM ionomycin and 5 mM $CaCl_2$. By integrating the traces in Origin 7 (OriginLab Corporation, Northampton, MA), the area under the curve was determined and expressed in arbitrary units.

To measure the free $[Ca^{2+}]_{ER}$, the cells were loaded with 20 μM MagFluo4-AM in Hepes-buffered saline (135 mM NaCl, 5.9 mM KCl, 11.6 mM Hepes, 1.5 mM $CaCl_2$, 11.5 mM glucose, 1.2 mM $MgCl_2$, pH 7.4) supplemented with 1 mg/ml of bovine serum albumin and 0.2 mg/ml of Pluronic F127 (Invitrogen) as described in Ref. 33. After 60 min, cells were permeabilized in Ca^{2+}-free cytosol-like medium containing 20 μg/ml of saponin (10 min at room temperature). Ca^{2+}-free cytosol-like medium had the following composition: 140 mM KCl, 20 mM NaCl, 1 mM EGTA, 2 mM $MgCl_2$, 20 mM Pipes, pH 7.0. Subsequently the solution was replaced with cytosol-like medium without Mg^{2+}, but supplemented with carbonyl cyanide 4-trifluoromethoxy-phenylhydrazone (10 μM) and 375 μM $CaCl_2$ to give a free $[Ca^{2+}]$ of 220 nM. 1.5 mM Mg-ATP was added at the beginning of each measurement to load the ER with Ca^{2+} via the sarcoplasmic/endoplasmic-reticulum Ca^{2+}-ATPase pumps. Upon reaching a maximal loading, IP_3 or ionomycin were added to the cells together with 10 μM TG to prevent re-uptake of Ca^{2+} into the ER. Results are calculated as F/F_0 of fluorescence emission at 525 nm after excitation at 490 nm.

Fluorescence was measured using a 96-well microplate reader equipped with automated fluid additions (FlexStation 3, Molecular Devices, Sunnyvale, CA). All experiments were performed at room temperature.

Confocal Imaging—Confocal images were made with an LSM510 confocal system on a Zeiss Axiovert 100M microscope (Carl Zeiss Meditec Inc., Jena, Germany) with a 488-nm argon and 543-nm HeNe laser. The ×40 plan neofluar, oil-immersion 1.3 NA, DIC objective was used. The images were analyzed with Zeiss LSM Software Release 4.2.

RESULTS

Full-length TRPP2 Interacts with Endogenous Full-length IP_3R1 or IP_3R3—To investigate whether full-length TRPP2 and the IP_3R directly interact in intact cells, we performed co-immunoprecipitation experiments (Fig. 1). An LLC-PK1 cell line stably expressing full-length wild-type TRPP2 was used. After cell lysis, immunoprecipitation was performed with an antibody against the C terminus of TRPP2. Specific association between TRPP2 and endogenous full-length IP_3R3 or IP_3R1 was detected by Western blotting analysis (Fig. 1*A*). The control experiment was performed with nonspecific mouse or rabbit IgG. Furthermore, when an antibody specifically against IP_3R1 or IP_3R3 was used for immunoprecipitation, we also identified TRPP2 in the precipitate by Western blotting analysis (Fig. 1*B*). Due to the insufficient quality of the antibodies available against IP_3R2, we could not detect or immunoprecipitate IP_3R2. The data in Fig. 1 indicate that TRPP2 interacts with both IP_3R1 and IP_3R3, the latter being the most abundant isoform in LLC-PK1 cells.

Interaction between TRPP2 and the N-terminal Ligand-binding Domain of the IP_3R1—Each of the four IP_3R monomers can be functionally divided in an N-terminal LBD that binds IP_3, a central regulatory/coupling domain and a C-terminal channel and gatekeeper domain (reviewed in Ref. 34). The N-terminal LBD (aa 1–604) can be functionally and structurally subdivided into a suppressor domain (aa 1–225) and an IP_3-binding core (aa 226–604) (35). A linear representation of the IP_3R is depicted in Fig. 2*A*. We have employed GST pulldown assays to further characterize the TRPP2-IP_3R interaction. To map the TRPP2-binding site on the IP_3R, we used a series of GST-IP_3R fusion proteins corresponding to five fragments covering the first N-terminal 2216 amino acids and 1 fragment corresponding to the last C-terminal 160 amino acids of mouse IP_3R1 (28, 29). These fragments are located in the cytoplasm and coincide with "natural" domains generated by limited proteolysis, but the transmembrane domain was not included (36). In addition to these six domains, we used a GST fusion protein covering the complete LBD (aa 1–604). After purification, the recombinant proteins migrated as prominent bands corresponding to their expected molecular weights (Fig. 2*B*). Lysates obtained from the LLC-PK1 cells stably expressing TRPP2 were incubated with the GST-IP_3R fragments pre-bound to glutathione-Sepharose 4B resin, with equal loading of the GST-IP_3R fragments. After pulldown and elution, the samples were processed by SDS-PAGE. TRPP2 was visualized using the mouse monoclonal antibody against TRPP2 (Fig. 2*B*). Full-length TRPP2 mainly interacted with the complete N-terminal LBD of the

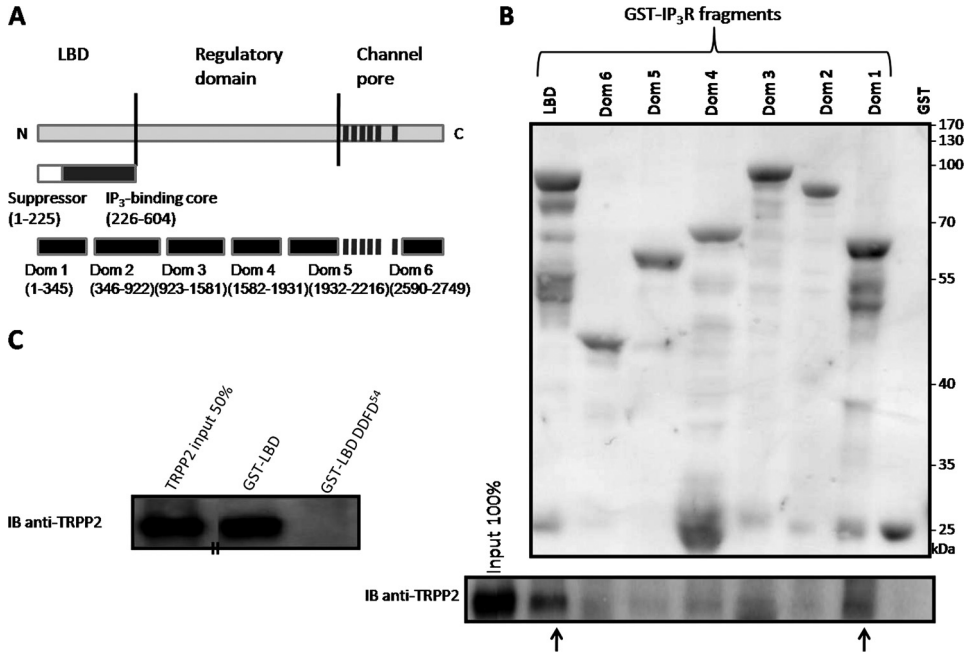

FIGURE 2. **GST pulldowns using purified IP_3R subdomains and full-length TRPP2.** *A,* linear structure of the IP_3R1: LBD, regulatory domain, and the channel pore. The LBD can be further divided into a suppressor domain (aa 1–225) and an IP_3-binding core (aa 226–604). GST is N-terminal fused to the LBD and to the six cytoplasmic domains of the IP_3R1. *B,* GST pulldown using the different domains of the IP_3R1, bacterially expressed and purified as GST fusion proteins, and full-length TRPP2, obtained from LLC-PK1 cells stably expressing TRPP2. The *upper panel* shows Ponceau red staining of the input proteins. The *lower* immunoblot shows the staining for TRPP2. The *arrows* indicate the bands with specific interaction. *C,* pulldown between GST-LBD or GST-LBD mutant ($KKFR^{54}$ is mutated to $DDFD^{54}$) and full-length TRPP2, obtained from LLC-PK1 cells stably expressing TRPP2. The immunoblot shows the staining for TRPP2. The *short parallel lines* indicates the position where a lane was moved from within the same blot.

IP_3R (aa 1–604) and with domain 1 (aa 1–345), which is part of this LBD (Fig. 2*B*, *lower panel*). The interaction was specific, as TRPP2 did not interact with the parental GST.

A Positively Charged Cluster in the Suppressor Region of the LBD of the IP_3R Interacts with an Acidic Cluster in the C-terminal Cytoplasmic Tail of TRPP2—Previous work in our laboratory identified a cluster of positively charged residues (aa 51–54) in the suppressor domain of the IP_3R1,[5] conserved among all three IP_3R isoforms, that were critical for interaction with negatively charged protein sequences, as *e.g.* in calmodulin (37). We therefore hypothesized that this positively charged cluster may be involved in the interaction with TRPP2, which contains a highly negatively charged cluster in the C-terminal cytoplasmic tail. We mutated two lysine residues and one arginine residue within this positive cluster to negatively charged aspartate residues ($KKFR^{54}$ to $DDFD^{54}$) in the GST-LBD construct (GST-LBD $DDFD^{54}$). Pulldown with GST fusion proteins of the LBD and the LBD $DDFD^{54}$ indicated that full-length TRPP2 could interact with GST-LBD but not with GST-LBD $DDFD^{54}$ (Fig. 2*C*).

Furthermore, an additional mutant of the LBD was made by mutating the three positively charged residues to neutral residues ($KKFR^{54}$ to $AAFA^{54}$) to avoid the too drastic structural changes that can occur by the mutations to negatively charged residues. To identify the region of TRPP2 required for interaction with IP_3R1, recombinant His_6 fusion proteins of the complete cytosolic N- (aa 1–221) (TRPP2-NT-HIS) and C-terminal part (aa 679–966) (TRPP2-CT-HIS) of TRPP2 were bacterially expressed and purified. Pulldown assays with GST-LBD and both GST-LBD mutants revealed a clear interaction between GST-LBD and TRPP2-CT (Fig. 3*A*). Like the full-length TRPP2, the interaction with GST-LBD $DDFD^{54}$ was abolished. Additionally, interaction with GST-LBD $AAFA^{54}$ was similarly abolished. In contrast to TRPP2-CT, TRPP2-NT could neither specifically interact with the LBD nor with its mutants (Fig. 3*A*), indicating that the C-terminal tail of TRPP2 is the major determinant for binding to the suppressor domain of the IP_3R. We then tested whether IP_3 could alter the interaction between the IP_3R and TRPP2, but this was not the case (supplemental Fig. S1). To confirm the interaction with both IP_3R1 and IP_3R3, a pulldown was performed between full-length TRPP2 or TRPP2-CT-HIS and the suppressor domains (aa 1–225) of IP_3R1 and IP_3R3, fused to GST (Fig. 3*B*). Both suppressor domains could pull down TRPP2, both full-length TRPP2 or only its C terminus. TRPP2-CT contains an acidic cluster (aa 810–818 SEEEDDEDS) located at the end of the ER retention signal, well conserved among chordates but absent in polycystin-2 like-1 (PKD2L1 or TRPP3) and -2 (PKD2L2 or TRPP5) (supplemental Fig. S2). A casein kinase 2-phosphorylation site (Ser^{810} in the mouse sequence, corresponding to Ser^{812} in the human sequence) is located within this cluster and has been shown to be important for channel regulation (25). This cluster is also involved in interactions with other proteins (20, 38). To test whether this acidic cluster is implicated in interaction with the IP_3R, peptides containing this cluster were synthesized. A peptide representing the acidic cluster (SLDDSEEEDDEDSGH) (AC), a phosphomimic mutant (SLDDDEEEDDEDSGH) (AC S810D), and a mutant peptide with four alanine mutations replacing the negatively charged amino acids (SLDDAEEAAAEDSGH) (AC mutant) were used in GST pulldown assays to compete for the interaction between TRPP2-CT-HIS and GST-LBD. As shown in Fig. 3*C*, increasing amounts of the AC peptide competed for binding of TRPP2-CT-HIS to GST-LBD. Also the phosphomimic peptide, which contains an extra negative charge, could clearly disrupt the interaction, even more effectively than the wild-type AC peptide (a residual binding of 18 *versus* 44%). The AC mutant peptide, which lacks several negative residues, did not interfere with the binding of TRPP2-CT-HIS to GST-LBD. We investigated further whether interaction was purely electrostatic or sequence-specific using a scrambled peptide of the acidic clus-

[5] B. Devogelaere, N. Nadif Kasri, E. Sammels, G. Bultynck, L. Missiaen, J. B. Parys, and H. De Smedt, unpublished results.

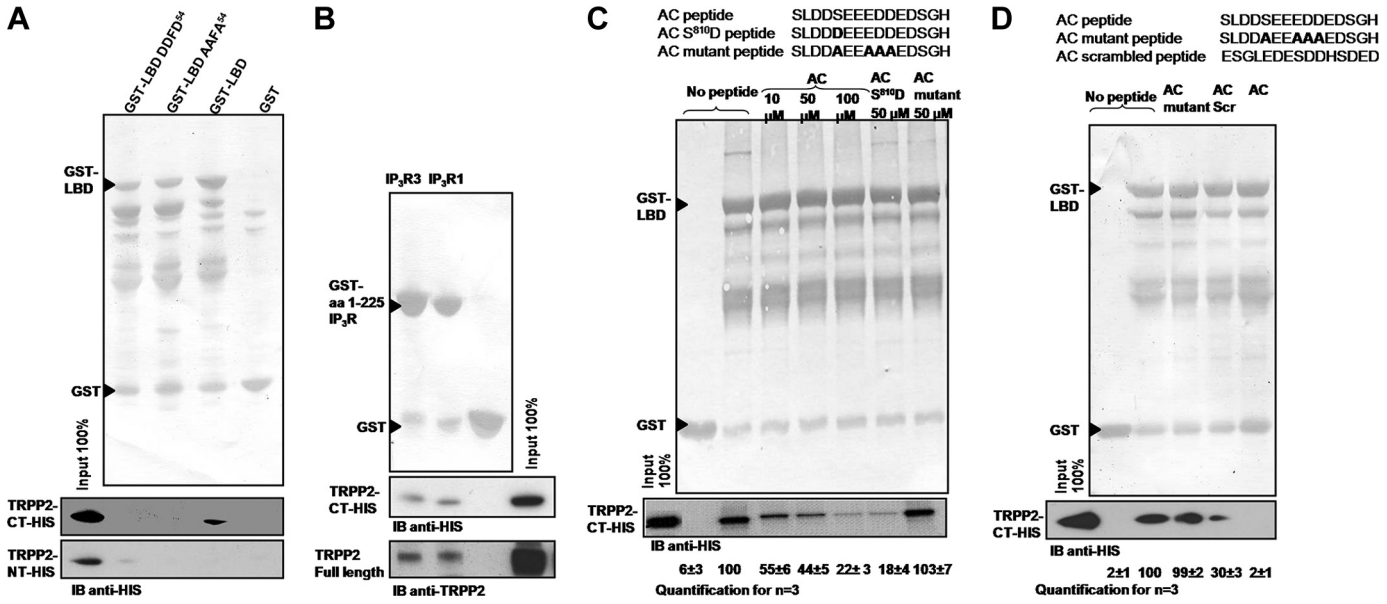

FIGURE 3. **Identification of the sequences involved in the interaction between TRPP2-CT and IP_3R-LBD.** *A,* GST pulldown using GST, GST-LBD, GST-LBD DDFD[54], or GST-LBD AAFA[54], and TRPP2-CT-HIS or TRPP2-NT-HIS. The *upper panel* shows Ponceau red staining of the input GST fusion proteins. The *lower* immunoblots show the staining for the HIS fusion proteins. *B,* GST pulldown using GST or GST-suppressor (aa 1–225) of IP_3R3 or IP_3R1 and full-length TRPP2 or TRPP2-CT-HIS. The *upper panel* shows Ponceau red staining of the input GST fusion proteins. The *lower* immunoblots show the staining for TRPP2-CT-HIS or full-length TRPP2. *C,* GST pulldown using GST-LBD and TRPP2-CT-HIS in the presence of acidic cluster peptide (*AC*) (10, 50, and 100 μM), the phosphomimic S810D peptide (*AC $S^{810}D$*) (50 μM), and the mutant peptide where four negatively charged residues are replaced by alanine (*AC mutant*) (50 μM). The *upper* immunoblot shows Ponceau red staining of the input proteins. The *lower* immunoblot shows the staining for TRPP2-CT-HIS. The quantification is averaged for three independent experiments and expressed in percent of the binding in the absence of peptides (mean ± S.E.). *D,* GST pulldown using GST-LBD and TRPP2-CT-HIS in the presence of 100 μM mutant acidic cluster peptide (*AC mutant*), scrambled acidic cluster peptide (*AC Scr*), and acidic cluster peptide itself (*AC*). The *upper* immunoblot shows Ponceau red staining of the input proteins. The *lower* immunoblot shows staining for TRPP2-CT-HIS. The quantification is averaged for three independent experiments and expressed in % of the binding in the absence of peptides (mean ± S.E.).

ter (AC Scr) in GST pulldown assays (Fig. 3*D*). Addition of the scrambled acidic cluster peptide resulted in partial disturbance of the interaction between GST-LBD and TRPP2-CT, however, to a much lesser extent than the acidic cluster peptide. This finding demonstrates that the interaction is primarily based on electrostatic charges but that the exact location of these charges is also important and leads to a sequence-specific effect. Taken together, these data indicate that the acidic cluster in the C-terminal tail of TRPP2 and the positively charged cluster in the suppressor domain of the IP_3R are crucial for interaction between the two proteins.

TRPP2 Potentiates ATP-induced Intracellular Ca^{2+} Release in Intact Cells—To study the effect of this molecular interaction on intracellular Ca^{2+} signaling, we used a $TRPP2^{-/-}$ renal epithelial cell line derived from $TRPP2^{-/WS25}$ mice (30) representing a zero-background system to study the effects mediated by wild-type TRPP2 or TRPP2 mutants. To re-introduce TRPP2 in these cells with high efficiency and an adjustable level of expression, we constructed an adenovirus encoding TRPP2. As shown on the Western blot and the confocal images (supplemental Fig. S3), the expression level of TRPP2 correlated with the virus titer. Adenoviral expressed TRPP2 was mainly localized in the ER. We chose a moderate TRPP2 expression, comparable with the endogenous levels of TRPP2 in renal epithelial cells (as shown in supplemental Fig. S4, *lanes 1* and *4*). This also excludes the need for making stable cell lines and the risk for concomitant selection of compensatory mutants. $TRPP2^{-/-}$ cells were transduced with a control virus or a TRPP2 virus to re-introduce wild-type TRPP2, and cultured in 96-well plates. In intact cells, we examined the intracellular Ca^{2+} release upon agonist (ATP) addition by monitoring the $[Ca^{2+}]_{cyt}$ in a microplate reader. Extracellular Ca^{2+} was buffered by addition of 3 mM EGTA at the beginning of each assay. For each ATP concentration (500 nM, 1 μM, and 10 μM), a significant potentiation of the Ca^{2+} release was observed in cells expressing TRPP2 compared with cells treated with the control virus (Fig. 4*A*, *black* and *red traces*). Both the amplitude (Fig. 4*B*) and the area under the curve (Fig. 4*C*) were significantly increased for all three ATP concentrations used. At a maximal dose of ATP (100 μM) there was, however, no longer a difference in Ca^{2+} release between the cells expressing TRPP2 compared with the cells treated with control virus (supplemental Fig. S5). The maximal releasable Ca^{2+} induced by 1 μM ionomycin was also not significantly altered (Fig. 4).

TRPP2 Potentiates IICR in Permeabilized Cells—The effect of TRPP2 on IICR was measured in plasma membrane-permeabilized cells loaded with the ER-resident Ca^{2+} indicator Mag-Fluo4. There was no significant difference in the loading of the ER with Ca^{2+} prior to the addition of IP_3 in cells treated with (i) a control virus, (ii) a TRPP2 virus, (iii) a TRPP2 D509V virus, and (iv) a TRPP2 R740X virus (discussed later) (supplemental Fig. S6). Therefore, the F/F_0 data were normalized by setting the maximal $[Ca^{2+}]_{ER}$ (as F/F_0) prior to the IP_3 addition at 100%.

TG (10 μM) alone was added to investigate whether TRPP2 could mediate a passive leak of Ca^{2+} from the ER. We could not detect a significant difference in the rate of $[Ca^{2+}]_{ER}$ decrease between control cells and cells expressing TRPP2 (Fig. 5*A*). Fur-

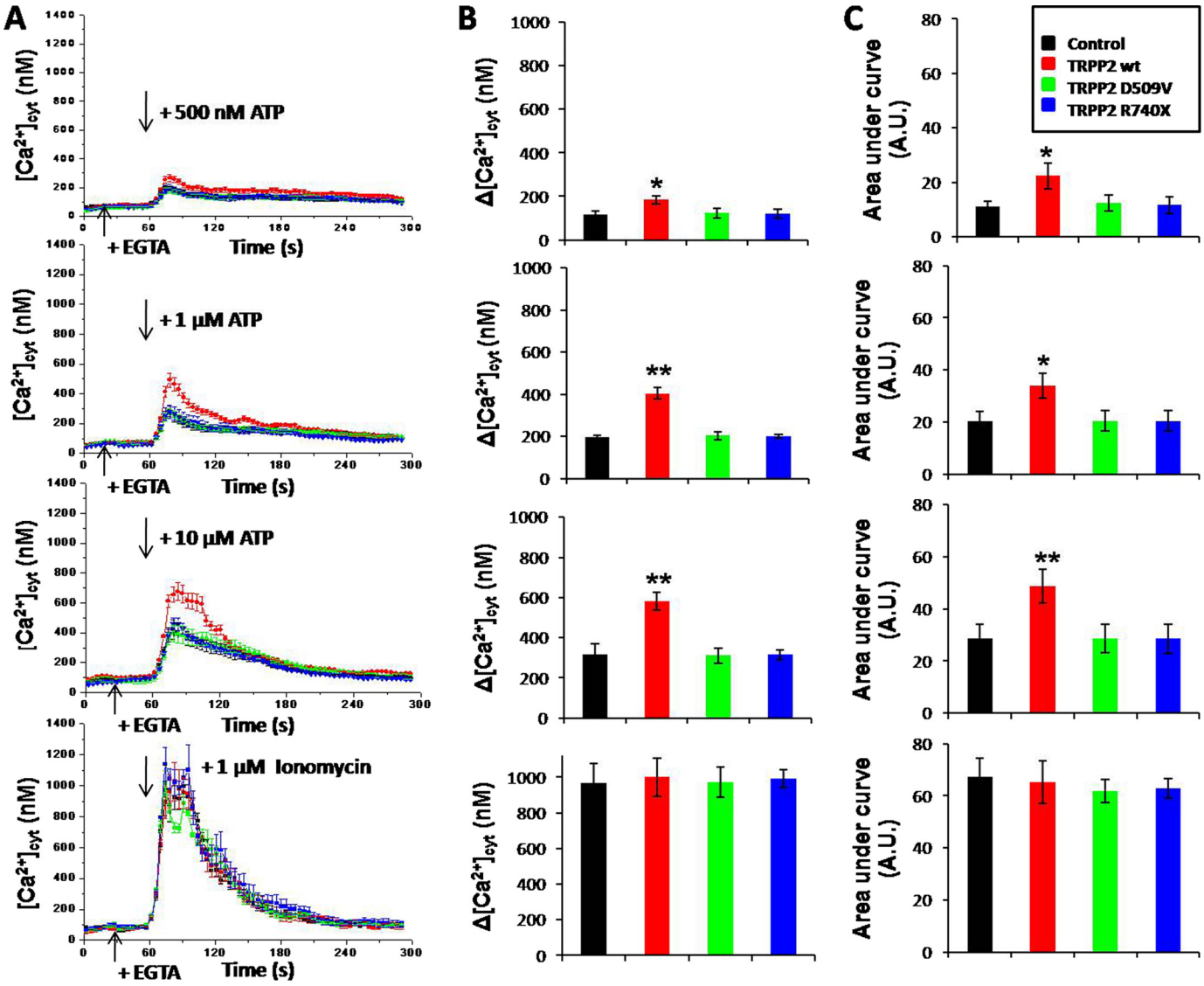

FIGURE 4. **Effect of TRPP2 and mutants on agonist-induced Ca^{2+} release in intact cells.** TRPP2$^{-/-}$ cells were treated with either control virus (*black*) (titer 1/1000) or a TRPP2 virus to re-introduce wild-type TRPP2 (*red*) (titer 1/1000) or mutants D509V (*green*) (titer 1/704) and R740X (*blue*) (titer 1/1124). The ratio of emitted fluorescence of Fura2 was monitored and the three different [ATP] or 1 μM ionomycin were added as indicated in the presence of 3 mM EGTA. $[Ca^{2+}]_{cyt}$ was derived after *in situ* calibration. *Panel A* shows the averaged traces of at least three independent experiments. *Panel B* shows the increase in $[Ca^{2+}]_{cyt}$ (nM) after agonist addition, averaged for at least three independent experiments. *Panel C* shows the quantification of the area under the curve in arbitrary units (*A.U.*). Results are shown as mean ± S.E. Statistically significant differences are labeled with: *, $p < 0.05$, and **, $p < 0.01$, using a Student's *t* test (paired two-tailed).

thermore, also in intact cells, we could not detect a significant difference in the rate of $[Ca^{2+}]_{cyt}$ rise between control cells and cells expressing TRPP2 (supplemental Fig. S7) and the maximal ER Ca^{2+} content was not changed (supplemental Fig. S7, 100 s). The maximal releasable Ca^{2+} in permeabilized cells, determined by adding 1 μM ionomycin, was the same for both conditions (Fig. 5*A*). However, TRPP2 potentiated IICR, because there was increased IICR in cells expressing TRPP2 compared with cells treated with the control virus (without TRPP2) when submaximal doses of IP_3 were applied (Fig. 5*B*). Application of a saturating dose of IP_3 (100 μM) no longer resulted in increased IICR in cells expressing TRPP2. A complete dose-response curve was fitted according to the Hill equation. The Hill coefficient and V_{max} remained unchanged, but the EC_{50} significantly changed from 5.77 ± 0.39 μM IP_3 in control cells to 3.09 ± 0.05 μM IP_3 in cells expressing TRPP2 ($p < 0.05$) (Table 1).

Stimulation of IICR Is Dependent on TRPP2-channel Function and Interaction with the IP_3R—To elucidate whether TRPP2 channel activity was involved in this effect on IICR, we made a D509V TRPP2 mutant. This pathological missense mutation of a single amino acid in the third membrane-spanning domain results in complete loss of TRPP2 channel activity (15). This mutant retained the ER localization and C-terminal-mediated protein interactions and regulatory domains. A second pathological R740X-truncated mutant, which lost the interaction site with the IP_3R, was made to verify whether the effect on IICR was dependent on the interaction between TRPP2 and IP_3R. This mutant still showed channel activity, although some channel properties like the regulation by Ca^{2+}

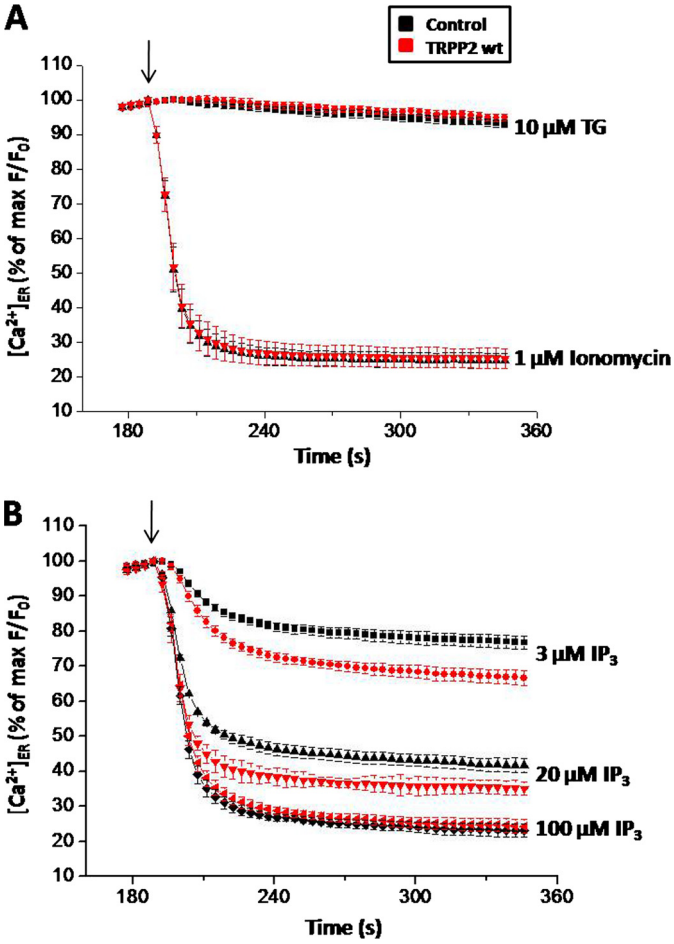

FIGURE 5. **Effect of TRPP2 on IP_3-induced Ca^{2+} release in permeabilized cells.** $TRPP2^{-/-}$ cells were treated with either a control virus (*black*) (titer 1/1000) or a TRPP2 virus (*red*) to re-introduce wild-type TRPP2 (titer 1/1000). The fluorescence signal (F/F_0) of the ER-resident Ca^{2+} indicator MagFluo4 was monitored. After permeabilizing the cells and loading the ER with Ca^{2+}, IP_3, TG, or ionomycin were applied as indicated. IP_3 was given in the presence of 10 μM TG to prevent re-uptake of Ca^{2+} into the ER. *Panel A* shows the $[Ca^{2+}]_{ER}$ (as % of max F/F_0) after application of 10 μM TG or 1 μM ionomycin. *Panel B* shows the $[Ca^{2+}]_{ER}$ (as % of max F/F_0) after application of 3, 20, or 100 μM IP_3. Mean ± S.E. of at least three independent experiments are shown.

TABLE 1

Fitting parameters according to the Hill equation of the IP_3 dose-response curves

Using 8 different IP_3 concentrations (250 and 500 nM, and 1, 3, 5, 20, 50, and 100 μM), a complete IP_3 dose-response curve for cells expressing wild-type TRPP2 or control cells was fitted according to the Hill equation. The parameters EC_{50}, Hill coefficient, and V_{max} are depicted. Results are shown as mean ± S.E. of three independent experiments.

	Control	TRPP2 wild-type	*p* value
EC50	5.77 ± 0.39	3.09 ± 0.05	0.016[a]
Hill coefficient	1.08 ± 0.09	1.15 ± 0.15	0.435
V_{max}	105.73 ± 5.11	103.22 ± 4.33	0.085

[a] Statistically significant differences with $p < 0.05$ using a Student's *t* test (paired two-tailed).

are altered, possibly due to loss of the EF-hand (15, 39). In supplemental Fig. S4, the adenoviral expression and subcellular localization of wild-type TRPP2 and the two mutants are shown on a Western blot and in confocal images. In contrast to wild-type TRPP2, none of the mutants potentiated intracellular Ca^{2+} release in intact cells upon addition of 500 nM, 1 μM, or 10 μM ATP compared with control cells (Fig. 4). The maximal releasable Ca^{2+} induced by 1 μM ionomycin was not significantly different.

Also in permeabilized cells, IICR was no longer potentiated in cells expressing the mutants as compared with wild-type TRPP2 (Fig. 6*A*). The decrease of the $[Ca^{2+}]_{ER}$ upon addition of 3 μM IP_3 is shown. This value amounted to 27.5 ± 2.1% in control cells, 38.9 ± 2.7% in TRPP2-expressing cells, 25.3 ± 1.4% in TRPP2 D509V-expressing cells, and 26.0 ± 1.2% in TRPP2 R740X expressing cells (Fig. 6*A*). The experiment with the channel-dead mutant indicates that the potentiation of IICR was dependent on TRPP2 channel activity. The results with the R740X mutant suggest also that the TRPP2-IP_3R interaction was needed for this potentiation of IICR, although it cannot be completely excluded that the loss of potentiation of IICR was due to altered TRPP2 channel properties. Therefore a second approach was used to validate the role of the interaction between TRPP2 and the IP_3R in intracellular Ca^{2+} signaling (Fig. 6*B*). Disruption of the interaction between TRPP2 and IP_3R by addition of the AC peptide (*cf.* Fig. 3*C*) prevented potentiation of IICR in TRPP2-expressing cells in response to 1 μM IP_3, whereas this potentiation was not prevented by AC mutant peptide (Fig. 6*B*). These peptides had no effect on IICR in control cells. These results confirm that an interaction between TRPP2 and IP_3R was required to potentiate intracellular Ca^{2+} release upon IP_3R activation.

We hypothesize that TRPP2 can be activated by an initial IICR via a Ca^{2+}-induced Ca^{2+}-release (CICR) mechanism. To substantiate this hypothesis, we used BAPTA, a faster Ca^{2+} buffer than EGTA, at a high concentration (20 mM BAPTA instead of 1 mM EGTA) in the Ca^{2+} assay in permeabilized cells. Under these conditions, TRPP2 no longer potentiated the IICR after addition of 5 μM IP_3 (Fig. 6*C*). It is noted that the extent of the release was lower when using BAPTA buffering, compared with EGTA buffering. The reason for this is that BAPTA can slightly inhibit IICR (40). To further rule out that TRPP2 did not simply function as an additional CICR mechanism but required an initial IICR, we applied submaximal doses of ionomycin in intact and permeabilized cells. This provoked a general rise in $[Ca^{2+}]_{cyt}$ and a decrease in $[Ca^{2+}]_{ER}$, but there was no potentiation of the Ca^{2+} release in cells expressing TRPP2, compared with cells treated with the control virus (Fig. 7). We therefore conclude that a local Ca^{2+} release as produced by IP_3 is required for inducing CICR via TRPP2, whereas a global Ca^{2+} increase as by ionomycin cannot produce this CICR.

Taken together, these data suggest that TRPP2 and the IP_3R form a signaling complex at the ER, thereby fine-tuning and coordinating Ca^{2+} signaling in a microdomain of intracellular Ca^{2+} release. The close proximity of TRPP2 channels and IP_3Rs in a protein complex thereby allows the amplification of IP_3R originating Ca^{2+} signals via a local CICR mechanism.

DISCUSSION

The main finding of this study was that endogenous TRPP2-IP_3R signaling complexes are responsible for the TRPP2-dependent potentiation of IICR. The novel findings in this work are: (i) the identification of residues responsible for the interaction, on TRPP2 as well as on the IP_3R, which can now be targeted to disrupt or enhance the interaction; (ii) the mechanism

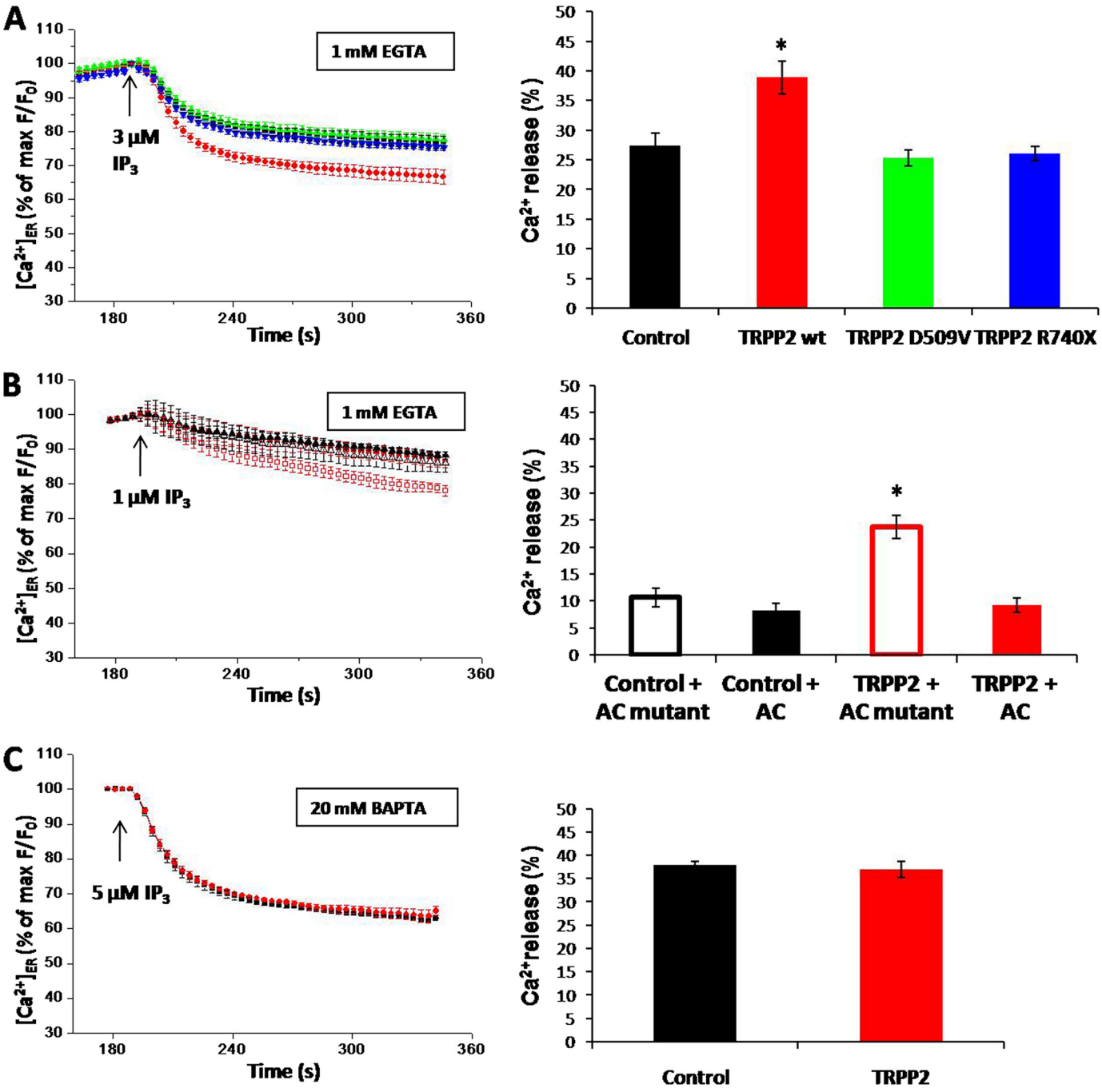

FIGURE 6. **Effect of TRPP2 mutants, competing peptides, and altered Ca^{2+} buffering conditions on IP_3-induced Ca^{2+} release in permeabilized cells.** *A*, $TRPP2^{-/-}$ cells were treated with either a control virus (*black*) (titer 1/1000) or a TRPP2 virus to re-introduce wild-type TRPP2 (*red*) (titer 1/1000) or mutants D509V (*green*) (titer 1/704) and R740X (*blue*) (titer 1/1124). Experiments were performed as described in the legend to Fig. 5 with 3 μM IP_3 and with 1 mM EGTA for Ca^{2+} buffering. *B*, $TRPP2^{-/-}$ cells were treated with either a control virus (*black*) (titer 1/1000) or a TRPP2 virus (*red*) to re-introduce wild-type TRPP2 (titer 1/1000) and assayed as described in the legend to Fig. 5. 1 μM IP_3 was added to the cells in the presence of 10 μM acidic cluster peptide (*AC*, *closed symbols*) or a mutant peptide (*AC mutant*, *open symbols*). Experiment was performed in the presence of 1 mM EGTA for Ca^{2+} buffering. *C*, $TRPP2^{-/-}$ cells were treated with either a control virus (*black*) (titer 1/1000) or a TRPP2 virus to re-introduce wild-type TRPP2 (*red*) (titer 1/1000). Experiments were performed as described in the legend to Fig. 5 with 5 μM IP_3, except that the Ca^{2+} was buffered with 20 mM BAPTA instead of 1 mM EGTA. The *left panels* show the results as mean $[Ca^{2+}]_{ER}$ (in % of max F/F_0) for at least three independent experiments. The *right panels* show the percentage Ca^{2+} release (mean ± S.E.). Data values were normalized to the ionomycin-induced Ca^{2+} release, which was taken as 100%, after subtracting the TG-induced Ca^{2+} release. Statistically significant differences are labeled with: *, $p < 0.05$, using a Student's *t* test (paired two-tailed).

responsible for the potentiated Ca^{2+} release, which was due to TRPP2 activity rather than to altered IP_3R activity and that required a close association between TRPP2 and the IP_3R to allow for a Ca^{2+} microdomain responsible for the activation of TRPP2; (iii) the finding that TRPP2 was not responsible for a passive Ca^{2+} leak from the ER; and (iv) the demonstration of CICR via TRPP2 in a cellular model. We conclude that an acidic cluster (aa 810–818) in the cytosolic C-terminal tail of TRPP2 and a positively charged cluster (aa 51–54) in the suppressor region of the LBD in the N terminus of the IP_3R were required

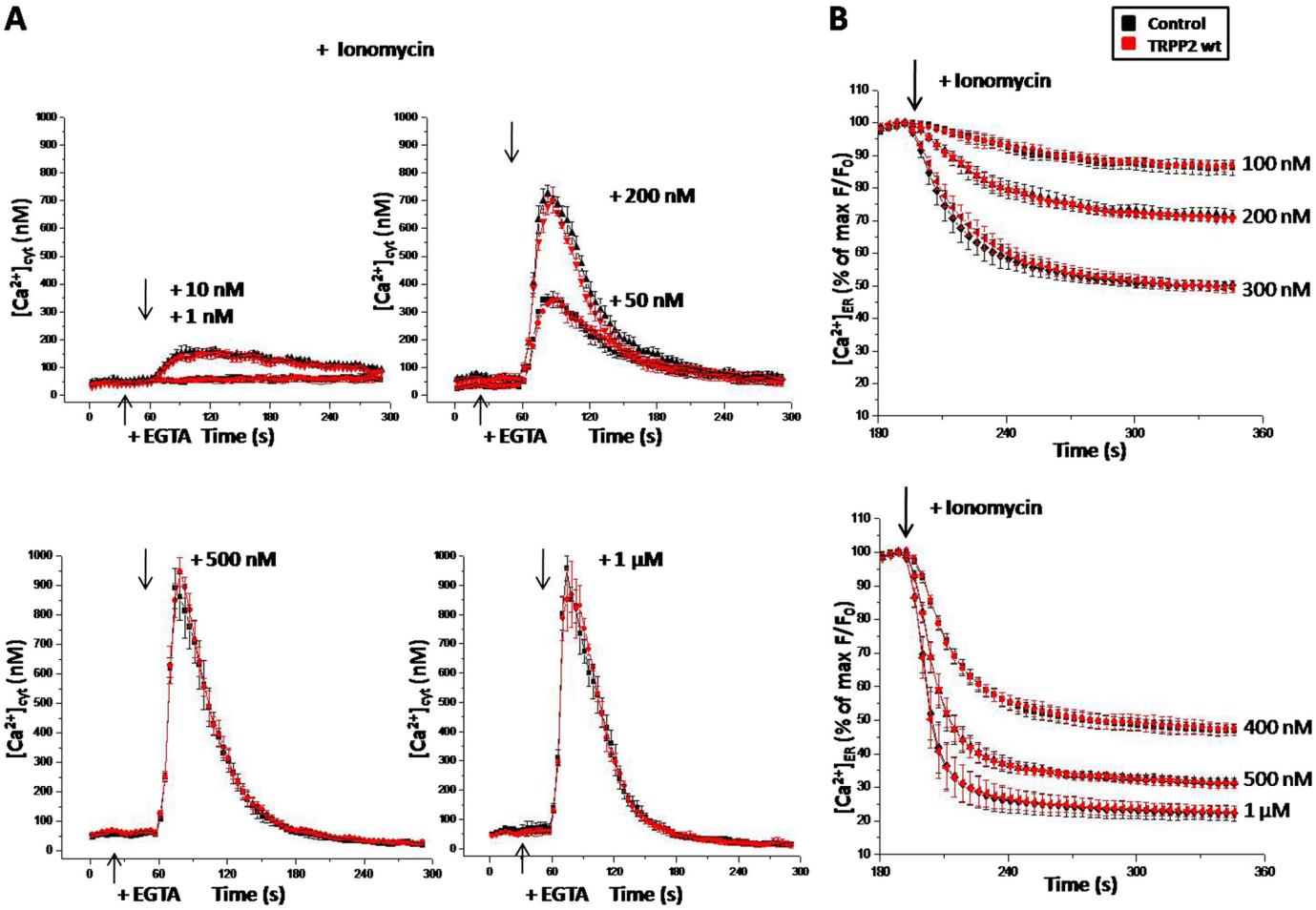

FIGURE 7. **Effect of TRPP2 on ionomycin-induced Ca^{2+} release in intact and permeabilized cells.** TRPP2$^{-/-}$ cells were treated with either control virus (*black*) (titer 1/1000) or a TRPP2 virus to re-introduce wild-type TRPP2 (*red*) (titer 1/1000). *A*, the ratio of emitted fluorescence of Fura2 was monitored and six different ionomycin concentrations were added as indicated in the presence of 3 mM EGTA. $[Ca^{2+}]_{cyt}$ was derived after *in situ* calibration. *Panel A* shows the averaged traces of at least three independent experiments. *B*, experiments were performed as described in the legend to Fig. 5 with the indicated ionomycin concentrations and with 1 mM EGTA for Ca^{2+} buffering. Results are shown as mean $[Ca^{2+}]_{ER}$ (as % of max F/F_0) ± S.E. for three independent experiments.

for their interaction. As a functional consequence of this interaction, we found that TRPP2 potentiated IICR. In a previous study (23) it was postulated that the C-terminal part of TRPP2 could alter the activity of the IP_3R. This conclusion was based on overexpression of the truncated C terminus or the channel-dead mutant in oocytes. Our data, however, do not provide evidence for a changed activity of the IP_3R as the channel-dead mutant of TRPP2 had no effect on IICR in our experimental model, where we have carefully avoided overexpression to physiologically irrelevant levels. Rather, the enhanced Ca^{2+} release was most likely due to activation of CICR via TRPP2. This was concluded from our observation that the potentiation of IICR by TRPP2 was abolished in strong Ca^{2+}-buffering conditions using 20 mM BAPTA, which reduces the microdomain of the elevated free $[Ca^{2+}]$ (41). The difference between slow (EGTA) or fast (BAPTA) Ca^{2+} buffering is an established method to estimate the importance of the local $[Ca^{2+}]_{cyt}$ rise in a microdomain close to Ca^{2+}-release channels. For this observed CICR, activation by a local $[Ca^{2+}]_{cyt}$ rise following IICR and the close proximity of the IP_3R via a direct interaction with TRPP2 appeared to be required. The latter was also evident from our observation that a truncated TRPP2, which lacks the IP_3R-binding site, did not provoke this potentiation of IICR. Moreover, the effect was also abolished by a peptide competing for the IP_3R-binding site. An additional support for the importance of a close interaction between TRPP2 and the IP_3R stems from the observation that a global $[Ca^{2+}]_{cyt}$ rise as provoked by ionomycin or TG did not result in an increased TRPP2-induced Ca^{2+} signal. We propose a model (Fig. 8) where upon cell stimulation IP_3 is produced and activates the IP_3R, which leads to a local $[Ca^{2+}]_{cyt}$ rise that subsequently can activate the TRPP2 channel as a CICR channel. Previous lipid-bilayer experiments have demonstrated regulation of the open probability of the TRPP2 channel by Ca^{2+} (25).

Besides important functions of TRPP2 at the plasma membrane and the primary cilia, we now suggest another critical function for TRPP2 in the ER. We propose the existence of a signaling microdomain that requires a functional TRPP2/IP_3R-protein complex to facilitate CICR by TRPP2. TRPP2 participates in an intracellular channel complex and potentiates intracellular IP_3-mediated Ca^{2+} signaling. It has been shown in lipid bilayer experiments that TRPP2 is a Ca^{2+}-dependent cation channel, whose activity shows a bell-shaped dependence on $[Ca^{2+}]_{cyt}$ (15, 25). The activation phase of the CICR via TRPP2 was reported to have micromolar affinity (25). Given the rela-

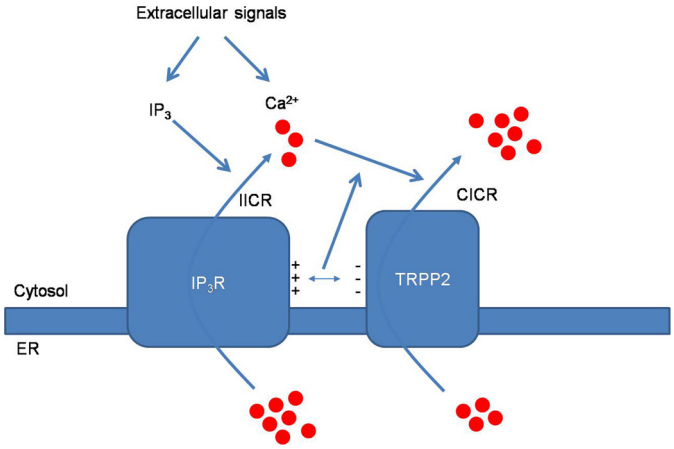

FIGURE 8. **Proposed model.** Upon cell stimulation, IP_3 is produced and activates the IP_3R leading to a local $[Ca^{2+}]_{cyt}$ rise that subsequently activates the TRPP2 channel as a CICR channel. We suggest that a signaling microdomain, where TRPP2 interacts with the IP_3R through the charged residues, is required to facilitate CICR by TRPP2.

tively high $[Ca^{2+}]$ predicted at the mouth of the IP_3R at the ER surface (34, 42), a micromolar affinity for Ca^{2+} may allow TRPP2 to sense such local changes in $[Ca^{2+}]_{cyt}$. Recent studies on the structure of the EF-hand within the cytosolic C terminus of TRPP2 have brought new insights into the conformational changes that occur upon Ca^{2+} binding (6, 8). However, the direct link between Ca^{2+} binding to the EF-hand of TRPP2 and its Ca^{2+}-dependent channel regulation has not been demonstrated yet and requires further research. Furthermore, loss of phosphorylation of TRPP2 (Ser^{810}) can shift the bell-shaped $[Ca^{2+}]_{cyt}$ dependence of TRPP2 channel activity to the right (25). Given our results from the binding assay with the phosphomimic acidic cluster peptide (Fig. 3*B*), reduced binding of TRPP2 to the IP_3R may be one of the mechanisms responsible for the observed decrease in sensitivity to Ca^{2+} upon dephosphorylation.

Intracellular Ca^{2+} signaling modulated by TRPP2 is important for regulating various cellular processes including cell proliferation. Loss of TRPP2 results in increased cell proliferation in ADPKD and this is one of the mechanisms leading to cyst formation (5, 43). It has been reported that ADPKD cystic cells have a lower $[Ca^{2+}]_{cyt}$, probably due to a loss of TRPP2 channel function (44). Increased levels of cAMP and cAMP-dependent genes (such as aquaporin 2) are also a common finding in the kidneys of different ADPKD animal models. In ADPKD or under Ca^{2+} deprivation conditions, cAMP stimulates cell proliferation in an Src-, Ras-, and B-Raf-dependent manner (45). In view of the role of Ca^{2+} in the regulation of cAMP metabolism via Ca^{2+}-inhibitable adenylyl cyclase 6 and/or via Ca^{2+}-dependent phosphodiesterase-1, it has already been suggested that alterations in intracellular Ca^{2+} homeostasis account for the increase in cAMP levels (5). It is tempting to speculate that the increased Ca^{2+} signaling in IP_3R/TRPP2 microdomains may be operative in controlling cellular cAMP levels by Ca^{2+} inhibitable adenylyl cyclases. Taken together, the previous findings strongly suggest that the mechanisms regulating $[Ca^{2+}]_{cyt}$ form potential therapeutic targets for ADPKD.

Not only proliferation, but also apoptosis is an important Ca^{2+}-regulated cellular process that is impaired in ADPKD, although this might be rather a consequence than a cause of cyst formation. Recently, Wegierski *et al.* (27) have proposed a role for ER-located TRPP2 in apoptosis. They have found that TRPP2 can lower the ER Ca^{2+} content, thereby protecting against apoptosis. In contrast to our data and previous work (15, 23), they observed that TRPP2 diminished cytosolic and mitochondrial Ca^{2+} signals induced by IP_3R activation. Because they observed a decreased ER Ca^{2+} content in TRPP2 overexpressing cells, it appeared that those cells have a diminished Ca^{2+} release upon IP_3R activation. In contrast, we could neither detect a change in $[Ca^{2+}]_{ER}$ nor in passive Ca^{2+} leak (Fig. 5*A* and supplemental Fig. S7), and we consistently observed an increase in IICR (Fig. 5*B*). A difference in our experimental cell model is that we did not overexpress TRPP2, but chose expression levels comparable with endogenous levels of TRPP2 (supplemental Fig. S4). In basal conditions, the TRPP2 channel is expected to be silent and inhibited by the endogenous protein syntaxin-5 (46). When TRPP2 is overexpressed, it is possible that the endogenous level of syntaxin-5 is not sufficient to maintain this basal inhibition of TRPP2.

In summary, we observed a clear interaction between TRPP2 and the IP_3R and identified a conserved positively charged cluster in the N-terminal suppressor domain of the IP_3R and an acidic cluster located at the end of the ER-retention signal in the C terminus of TRPP2 as being crucial for their interaction. When full-length TRPP2 was re-introduced in $TRPP2^{-/-}$ mouse renal epithelial cells, there was a clear potentiation of agonist-induced intracellular Ca^{2+} release in intact cells and IICR in permeabilized cells. Further analysis using pathological mutants of TRPP2 and competing peptides revealed that this effect on IICR was dependent on the TRPP2 channel function and on the interaction with the IP_3R. We propose a model in which the TRPP2 channel itself is activated as a CICR channel by a local $[Ca^{2+}]_{cyt}$ rise generated by IICR (Fig. 8).

We conclude that a signaling complex involving TRPP2 and the IP_3R is important for modulating intracellular Ca^{2+} signaling. Disturbance of this interaction, which occurs in pathologically relevant mutants of TRPP2, will lead to altered intracellular Ca^{2+} homeostasis and might contribute to the development of ADPKD caused by loss-of-function mutations in TRPP2.

Acknowledgments—We are grateful for excellent technical assistance by Tomas Luyten, Irène Willems, and Wendy Janssens. We thank Dr. N. Nadif Kasri for making the polycystin-2 overexpressing LLC-PK1 cell line. We are grateful to Dr. B. Ehrlich, Yale University, New Haven, CT, for fruitful discussions. We thank Dr. V. Gerke, University of Münster, Germany, for the cDNA clone of TRPP2. We thank Dr. B. Nilius and Dr. T. Voets, K. U. Leuven, for carefully reading and commenting on this manuscript.

REFERENCES

1. Gabow, P. A., and Grantham, J. J. (1997) in *Diseases of the Kidney* (Schrier, R. W., and Gottschalk, C. W., eds) 6th Ed., pp 521–560, Little Brown and Company, Boston, MA
2. Mochizuki, T., Wu, G., Hayashi, T., Xenophontos, S. L., Veldhuisen, B., Saris, J. J., Reynolds, D. M., Cai, Y., Gabow, P. A., Pierides, A., Kimberling, W. J., Breuning, M. H., Deltas, C. C., Peters, D. J., and Somlo, S. (1996)

Science **272,** 1339–1342
3. Harris, P. C. (2009) *J. Am. Soc. Nephrol.* **20,** 1188–1198
4. Wu, G., and Somlo, S. (2000) *Mol. Genet. Metab.* **69,** 1–15
5. Torres, V. E., and Harris, P. C. (2009) *Kidney Int.* **76,** 149–168
6. Schumann, F., Hoffmeister, H., Bader, R., Schmidt, M., Witzgall, R., and Kalbitzer, H. R. (2009) *J. Biol. Chem.* **284,** 24372–24383
7. Cai, Y., Maeda, Y., Cedzich, A., Torres, V. E., Wu, G., Hayashi, T., Mochizuki, T., Park, J. H., Witzgall, R., and Somlo, S. (1999) *J. Biol. Chem.* **274,** 28557–28565
8. Celić, A., Petri, E. T., Demeler, B., Ehrlich, B. E., and Boggon, T. J. (2008) *J. Biol. Chem.* **283,** 28305–28312
9. Yu, Y., Ulbrich, M. H., Li, M. H., Buraei, Z., Chen, X. Z., Ong, A. C., Tong, L., Isacoff, E. Y., and Yang, J. (2009) *Proc. Natl. Acad. Sci. U.S.A.* **106,** 11558–11563
10. Hanaoka, K., Qian, F., Boletta, A., Bhunia, A. K., Piontek, K., Tsiokas, L., Sukhatme, V. P., Guggino, W. B., and Germino, G. G. (2000) *Nature* **408,** 990–994
11. Nauli, S. M., Alenghat, F. J., Luo, Y., Williams, E., Vassilev, P., Li, X., Elia, A. E., Lu, W., Brown, E. M., Quinn, S. J., Ingber, D. E., and Zhou, J. (2003) *Nat. Genet.* **33,** 129–137
12. Tsiokas, L., Arnould, T., Zhu, C., Kim, E., Walz, G., and Sukhatme, V. P. (1999) *Proc. Natl. Acad. Sci. U.S.A.* **96,** 3934–3939
13. Bai, C. X., Giamarchi, A., Rodat-Despoix, L., Padilla, F., Downs, T., Tsiokas, L., and Delmas, P. (2008) *EMBO Rep.* **9,** 472–479
14. Köttgen, M., Buchholz, B., Garcia-Gonzalez, M. A., Kotsis, F., Fu, X., Doerken, M., Boehlke, C., Steffl, D., Tauber, R., Wegierski, T., Nitschke, R., Suzuki, M., Kramer-Zucker, A., Germino, G. G., Watnick, T., Prenen, J., Nilius, B., Kuehn, E. W., and Walz, G. (2008) *J. Cell Biol.* **182,** 437–447
15. Koulen, P., Cai, Y., Geng, L., Maeda, Y., Nishimura, S., Witzgall, R., Ehrlich, B. E., and Somlo, S. (2002) *Nat. Cell Biol.* **4,** 191–197
16. Tsiokas, L., Kim, S., and Ong, E. C. (2007) *Cell Signal.* **19,** 444–453
17. Giamarchi, A., Padilla, F., Coste, B., Raoux, M., Crest, M., Honoré, E., and Delmas, P. (2006) *EMBO Rep.* **7,** 787–793
18. Köttgen, M. (2007) *Biochim. Biophys. Acta* **1772,** 836–850
19. Geng, L., Okuhara, D., Yu, Z., Tian, X., Cai, Y., Shibazaki, S., and Somlo, S. (2006) *J. Cell Sci.* **119,** 1383–1395
20. Köttgen, M., Benzing, T., Simmen, T., Tauber, R., Buchholz, B., Feliciangeli, S., Huber, T. B., Schermer, B., Kramer-Zucker, A., Höpker, K., Simmen, K. C., Tschucke, C. C., Sandford, R., Kim, E., Thomas, G., and Walz, G. (2005) *EMBO J.* **24,** 705–716
21. Köttgen, M., and Walz, G. (2005) *Pflugers Arch.* **451,** 286–293
22. Anyatonwu, G. I., Estrada, M., Tian, X., Somlo, S., and Ehrlich, B. E. (2007) *Proc. Natl. Acad. Sci. U.S.A.* **104,** 6454–6459
23. Li, Y., Wright, J. M., Qian, F., Germino, G. G., and Guggino, W. B. (2005) *J. Biol. Chem.* **280,** 41298–41306
24. Li, Y., Santoso, N. G., Yu, S., Woodward, O. M., Qian, F., and Guggino, W. B. (2009) *J. Biol. Chem.* **284,** 36431–36441
25. Cai, Y., Anyatonwu, G., Okuhara, D., Lee, K. B., Yu, Z., Onoe, T., Mei, C. L., Qian, Q., Geng, L., Wiztgall, R., Ehrlich, B. E., and Somlo, S. (2004) *J. Biol. Chem.* **279,** 19987–19995
26. Miyagi, K., Kiyonaka, S., Yamada, K., Miki, T., Mori, E., Kato, K., Numata, T., Sawaguchi, Y., Numaga, T., Kimura, T., Kanai, Y., Kawano, M., Wakamori, M., Nomura, H., Koni, I., Yamagishi, M., and Mori, Y. (2009) *J. Biol. Chem.* **284,** 34400–34412
27. Wegierski, T., Steffl, D., Kopp, C., Tauber, R., Buchholz, B., Nitschke, R., Kuehn, E. W., Walz, G., and Köttgen, M. (2009) *EMBO J.* **28,** 490–499
28. Lee, B., Vermassen, E., Yoon, S. Y., Vanderheyden, V., Ito, J., Alfandari, D., De Smedt, H., Parys, J. B., and Fissore, R. A. (2006) *Development* **133,** 4355–4365
29. Sienaert, I., Missiaen, L., De Smedt, H., Parys, J. B., Sipma, H., and Casteels, R. (1997) *J. Biol. Chem.* **272,** 25899–25906
30. Wu, G., D'Agati, V., Cai, Y., Markowitz, G., Park, J. H., Reynolds, D. M., Maeda, Y., Le, T. C., Hou, H., Jr., Kucherlapati, R., Edelmann, W., and Somlo, S. (1998) *Cell* **93,** 177–188
31. Grimm, D. H., Cai, Y., Chauvet, V., Rajendran, V., Zeltner, R., Geng, L., Avner, E. D., Sweeney, W., Somlo, S., and Caplan, M. J. (2003) *J. Biol. Chem.* **278,** 36786–36793
32. Parys, J. B., De Smedt, H., Missiaen, L., Bootman, M. D., Sienaert, I., and Casteels, R. (1995) *Cell Calcium* **17,** 239–249
33. Laude, A. J., Tovey, S. C., Dedos, S. G., Potter, B. V., Lummis, S. C., and Taylor, C. W. (2005) *Cell Calcium* **38,** 45–51
34. Foskett, J. K., White, C., Cheung, K. H., and Mak, D. O. (2007) *Physiol. Rev.* **87,** 593–658
35. Devogelaere, B., Verbert, L., Parys, J. B., Missiaen, L., and De Smedt, H. (2008) *Cell Calcium* **43,** 17–27
36. Yoshikawa, F., Iwasaki, H., Michikawa, T., Furuichi, T., and Mikoshiba, K. (1999) *J. Biol. Chem.* **274,** 316–327
37. Kasri, N. N., Bultynck, G., Smyth, J., Szlufcik, K., Parys, J. B., Callewaert, G., Missiaen, L., Fissore, R. A., Mikoshiba, K., and De Smedt, H. (2004) *Mol. Pharmacol.* **66,** 276–284
38. Li, X., Luo, Y., Starremans, P. G., McNamara, C. A., Pei, Y., and Zhou, J. (2005) *Nat. Cell Biol.* **7,** 1202–1212
39. Chen, X. Z., Segal, Y., Basora, N., Guo, L., Peng, J. B., Babakhanlou, H., Vassilev, P. M., Brown, E. M., Hediger, M. A., and Zhou, J. (2001) *Biochem. Biophys. Res. Commun.* **282,** 1251–1256
40. Richardson, A., and Taylor, C. W. (1993) *J. Biol. Chem.* **268,** 11528–11533
41. Hay, J. C. (2007) *EMBO Rep.* **8,** 236–240
42. Neher, E. (1998) *Neuron* **20,** 389–399
43. Chang, M.-Y., and Ong, A. C. (2008) *Nephron Physiol.* **108,** 1–7
44. Yamaguchi, T., Hempson, S. J., Reif, G. A., Hedge, A. M., and Wallace, D. P. (2006) *J. Am. Soc. Nephrol.* **17,** 178–187
45. Yamaguchi, T., Nagao, S., Wallace, D. P., Belibi, F. A., Cowley, B. D., Pelling, J. C., and Grantham, J. J. (2003) *Kidney Int.* **63,** 1983–1994
46. Geng, L., Boehmerle, W., Maeda, Y., Okuhara, D. Y., Tian, X., Yu, Z., Choe, C. U., Anyatonwu, G. I., Ehrlich, B. E., and Somlo, S. (2008) *Proc. Natl. Acad. Sci. U.S.A.* **105,** 15920–15925